O-spline FIR filters for obtaining the Synchrophasor of Real Signals

José Antonio de la O Serna
Universidad Autónoma de Nuevo León
Monterrey, N. L., México

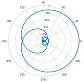

The 2nd IEEE International Conference on Smart Grid Synchronized Measurements and Analytics (SGSMA)
Virtual Event May 24-27, 2021

Co-authors in DTTFT Papers

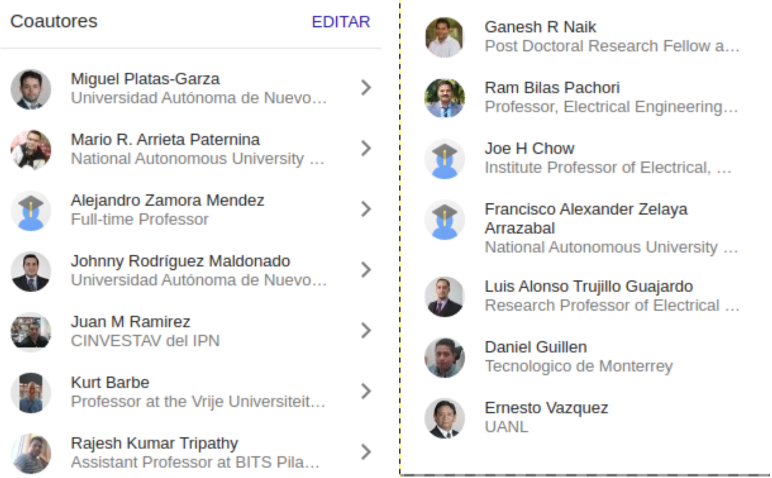

Figure 1: Coauthors in DTTFT design or applications papers (Wendy Van Moer).

Outline

Introduction I

- Splines are polynomial piecewise functions used normally in interpolation.
- A new kind of splines is presented: the O-splines[1].
- Odd order O-splines are cardinal splines: continuous functions of compact support with zero crossings at their knots.
- They are used here as bandpass filters to analyze oscillations.
- They converge to the ideal filter as the order $K \to \infty$.
- In interpolation, odd order O-splines correspond with the Lagrange central interpolation kernel of the same order. However, the Schoenberg interpolation splines are longer than O-splines [2].

[1] J. A. de la O Serna, "Dynamic Harmonic Analysis with FIR filters designed with O-splines", *IEEE Transactions on Circuits and Systems I: Regular Papers*, Vol.67, No.12, Dec. 2020, pp. 5092-5100.

[2] E. Meijering, W. J. Niessen, M. A. Viergever, The Sinc-approximating kernels of classical polynomial interpolation, IEEE International Conference on Image Processing-ICIP 99.

Introduction II

- O-splines in closed-form reduce the computational complexity of the DTTFT.
- In addition, O-splines come with their derivatives that perform as ideal differentiators.
- They provide a sequence of adjustable FIR filters that offer optimal coefficients for Hermite interpolation of the approximated function.
- They are very useful for multi-resolution and time-frequency analysis.

Signal Model

The complete response of a linear system due to a singularity of multiplicity $K+1$ at $s_h = -\sigma_h + j\omega_h$ is of the form:

$$x(t) = (c_K t^K + c_{K-1} t^{K-1} + \ldots + c_0) e^{-\sigma_h t} e^{j\omega_h t} \tag{1}$$

which corresponds to $Res\{H(s)e^{st}\}|_{s_h}$.

- **Fourier** signal model is the poorest one, since it assumes single singularities at harmonic frequencies: $c_h e^{jh\omega_1 t}, h \in \mathcal{Z}$.
- **Prony** signal model adds attenuation to the former one: $c_h e^{-\sigma_h t} e^{j\omega_h t}$.
- **Taylor-Fourier** signal model is the most complete, since it assumes repeated singularities: $(c_K t^K + c_{K-1} t^{K-1} + \ldots + c_0) e^{-\sigma_h t} e^{j\omega_h t}$

DTTFT signal model

The signal model of DTTFT is:

$$x(t) = \sum_{h=-\infty}^{\infty} \xi_h(t) e^{j2\pi h f_1 t}, \qquad -C\frac{T_1}{2} \leq t \leq C\frac{T_1}{2}. \quad (2)$$

where $\xi_h(t) \in \mathbb{C}$ is the h-th *complex envelope or dynamic phasor*, that replace the static *Fourier coefficient* of DFT. Each one of these functions are approached by a K-th Taylor expansion of the form

$$\xi_h^{(K)}(t) = \xi_h(t_0) + \dot{\xi}_h(t_0)t + \cdots + \overset{(K)}{\dot{\xi}}_h(t_0)\frac{t^K}{K!} \quad (3)$$

where the coefficients $\overset{(k)}{\dot{\xi}}_h(t_0) \in \mathbb{C}$ are the k-th derivatives of complex envelope $\xi_h(t)$, corresponding to the h-th harmonic frequency in (2). The time evolution of these coefficients perform as *state spectrograms* of $x(t)$.

Signal Model: Synthesis Equation

$$
\begin{aligned}
x_K &= \Phi_K \xi_K \\
&= \left(I \begin{pmatrix} W_N \\ W_N \\ \vdots \\ W_N \end{pmatrix} \quad T \begin{pmatrix} W_N \\ W_N \\ \vdots \\ W_N \end{pmatrix} \quad \cdots \quad \frac{1}{K!} T^K \begin{pmatrix} W_N \\ W_N \\ \vdots \\ W_N \end{pmatrix} \right) \begin{pmatrix} \xi_N \\ \dot{\xi}_N \\ \vdots \\ \xi^{(K)}_N \end{pmatrix}
\end{aligned}
\tag{4}
$$

where N is the number of samples per fundamental cycle, and K is the order of the Taylor expansion.

Solution: Analysis Equation

$$\widehat{\xi} = \widetilde{\Phi}^H x \tag{5}$$

where $\widetilde{\Phi}$ is the dual matrix given by

$$\widetilde{\Phi} = \Phi(\Phi^H \Phi)^{-1} \tag{6}$$

such that $\widetilde{\Phi}^H \Phi = I$. Notice $\widetilde{\Phi}^H$ is the inverse of Φ.

Factorization

$$
\begin{aligned}
\Phi_K &= \Upsilon_K \Omega_K \\
&= \begin{pmatrix} I & T_1 & \dots & \frac{1}{K!} T_1^K \\ I & T_2 & \dots & \frac{1}{K!} T_2^K \\ \vdots & \vdots & \ddots & \vdots \\ I & T_C & \dots & \frac{1}{K!} T_C^K \end{pmatrix} \begin{pmatrix} W_N & 0 & \dots & 0 \\ 0 & W_N & \dots & 0 \\ \vdots & \vdots & \ddots & \vdots \\ 0 & 0 & \dots & W_N \end{pmatrix}
\end{aligned} \tag{7}
$$

Its dual is

$$
\widetilde{\Phi} = \Upsilon(\Upsilon^H \Upsilon)^{-1} \frac{\Omega}{N} = \widetilde{\Upsilon} \frac{\Omega}{N}, \tag{8}
$$

with

$$
\widetilde{\Upsilon} = \Upsilon^{-T}. \tag{9}
$$

In consequence

$$
\widetilde{\Upsilon} = \frac{Adj(\Upsilon)^T}{|\Upsilon|} = \frac{Cof(\Upsilon)}{|\Upsilon|}. \tag{10}
$$

Key Idea for the Solution ($K = 1$)

For $K = 1$, $t_1 = t_{[-T_1,0)}$, and $t_2 = t_{[0,T_1)} = t_1 + T_1$, we have

$$\Phi_0^{(1)} = \begin{pmatrix} 1 & t_1 \\ 1 & t_2 \end{pmatrix} \tag{11}$$

with $|\Phi_0^{(1)}| = t_2 - t_1 = T_1$. Then, we have:

$$\widetilde{\Phi}_0^{(1)} = \frac{\begin{pmatrix} t_2 & -1 \\ -t_1 & 1 \end{pmatrix}}{T_1} = \begin{pmatrix} u_1 + 1 & -F_1 \\ -(u_2 - 1) & +F_1 \end{pmatrix} \tag{12}$$

where u_n is the normalized time: $u = t_n / T_1$. Its columns are a triangular pulse:

$$\widetilde{\varphi}_0^{(1)}(u) = \begin{cases} u + 1 & \text{for} \quad -1 \leq u < 0, \\ 1 - u & \text{for} \quad 0 \leq u < 1, \\ 0 & \text{otherwise}, \end{cases} \tag{13}$$

and the scaled Haar wavelet: $-F_1 \dot{\widetilde{\varphi}}_0^{(1)}(u)$.

Key idea for the solution ($K = 2$)

For $K = 2$, we have

$$\Phi_0^{(2)} = \begin{pmatrix} 1 & t_1 & t_1^2/2 \\ 1 & t_2 & t_2^2/2 \\ 1 & t_3 & t_3^2/2 \end{pmatrix}. \tag{14}$$

with $t_1 = t_{[-\frac{3T_1}{2}, -\frac{T_1}{2})}$, $t_2 = t_1 + T_1$, and $t_3 = t_1 + 2T_1$. In this case $|\Phi_0^{(2)}| = T_1^3$, and

$$\widetilde{\Phi}_0^{(2)} = \begin{pmatrix} \frac{1}{2}(u_1+2)(u_1+1) & -F_1(u_1+\frac{3}{2}) & F_1^2 \\ -(u_2+1)(u_2-1) & 2F_1u_2 & -2F_1^2 \\ \frac{1}{2}(u_3-1)(u_3-2) & -F_1(u_3-\frac{3}{2}) & F_1^2 \end{pmatrix}. \tag{15}$$

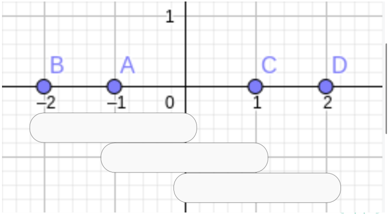

Key Idea ($K = 3$)

Finally, for $K = 3$, $t_1 = t_{[-2T_1, -T_1)}$ and $t_n = t_1 + (n-1)T_1 \;\; n = 2, 3, 4$.
We have $|\Phi_0^{(3)}| = T_1^6$. Its first dual column is:

$$\tilde{\varphi}_0^{(3)}(u) = \begin{cases} \frac{1}{6}(u+3)(u+2)(u+1) & \text{for} -2 \leq u < -1, \\ -\frac{1}{2}(u+2)(u+1)(u-1) & \text{for} -1 \leq u < 0, \\ \frac{1}{2}(u+1)(u-1)(u-2) & \text{for} \quad 0 \leq u < 1, \\ -\frac{1}{6}(u-1)(u-2)(u-3) & \text{for} \quad 1 \leq u < 2, \\ 0 & \text{otherwise.} \end{cases} \tag{16}$$

and the following ones are: $-F_1\dot{\tilde{\varphi}}_0^{(3)}$, $F_1^2\ddot{\tilde{\varphi}}_0^{(3)}$, and $-F_1^3\dddot{\tilde{\varphi}}_0^{(3)}$.
O-splines are recognized as the *Lagrange central interpolation kernels.*

O-splines and derivatives up to $K = 3$.

.

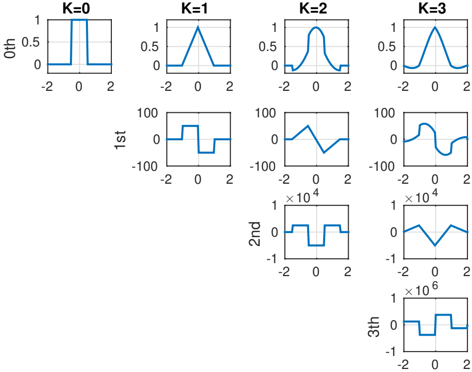

Figure 3: At the top, the O-splines of order K, for $K = 0, 1, 2, 3$, below each one of them its successive derivatives.

O-splines are stable functions or Multiresolution Analysis (MRA) *generators*

If $\varphi(u) \in V_0$, the set of integer translates $\{\varphi(u-n)\}_{n \in \mathcal{Z}}$ is an *inconditional basis* (or Riesz basis) of V_0, and forms a Multiresolution Analysis on $\mathcal{R}$.

O-splines Relationships

$$\varphi^0(u) = \begin{cases} 1 & \text{for } -\frac{1}{2} \leq u \leq \frac{1}{2} \\ 0 & \text{otherwise} \end{cases} \tag{17}$$

The first O-spline

$$\varphi^1(u) = \begin{cases} u+1 & \text{for } -1 \leq u \leq 0 \\ -(u-1) & \text{for } 0 \leq u \leq 1 \\ 0 & \text{otherwise} \end{cases} \tag{18}$$

and its first derivative:

$$\dot{\varphi}^1(u) = f_0(\varphi^0(u+\frac{1}{2}) - \varphi^0(u-\frac{1}{2})) \tag{19}$$

O-splines Relationships

The second O-spline

$$\varphi^2(u) = \begin{cases} \frac{1}{2}(u+2)(u+1) & \text{for } -\frac{3}{2} \le u \le -\frac{1}{2} \\ -(u+1)(u-1) & \text{for } -\frac{1}{2} \le u \le \frac{1}{2} \\ \frac{1}{2}(u-1)(u-2) & \text{for } \frac{1}{2} \le u \le \frac{3}{2} \\ 0 & \text{otherwise,} \end{cases} \tag{20}$$

its first derivative:

$$\dot{\varphi}^2(u) = f_0(\varphi^1(u+\frac{1}{2}) - \varphi^1(u-\frac{1}{2})), \tag{21}$$

and its second derivative:

$$\ddot{\varphi}^2(u) = f_0^2(\varphi^0(u+1) - 2\varphi^0(u) + \varphi^0(u-1)). \tag{22}$$

O-splines Relationships

And finally the third O-spline:

$$\varphi^3(u) = \begin{cases} \frac{1}{6}(u+3)(u+2)(u+1) & \text{for } -2 \leq u \leq -1 \\ -\frac{1}{2}(u+2)(u+1)(u-1) & \text{for } -1 \leq u \leq 0 \\ \frac{1}{2}(u+1)(u-1)(u-2) & \text{for } 0 \leq u \leq 1 \\ -\frac{1}{6}(u-1)(u-2)(u-3) & \text{for } 1 \leq u \leq 2 \\ 0 & \text{otherwise,} \end{cases} \tag{23}$$

its first derivative:

$$\dot{\varphi}^3(u) = f_0(\varphi^2(u+\frac{1}{2}) - \varphi^2(u-\frac{1}{2})), \tag{24}$$

its second derivative:

$$\ddot{\varphi}^3(u) = f_0^2(\varphi^1(u+1) - 2\varphi^1(u) + \varphi^1(u-1)) \tag{25}$$

and, finally its third derivative:

$$\dddot{\varphi}^3(u) = f_0^3(\varphi^0(u+\frac{3}{2}) - 3\varphi^0(u+\frac{1}{2}) + 3\varphi^0(u-\frac{1}{2}) - \varphi^0(u-\frac{3}{2})) \tag{26}$$

101st O-spline

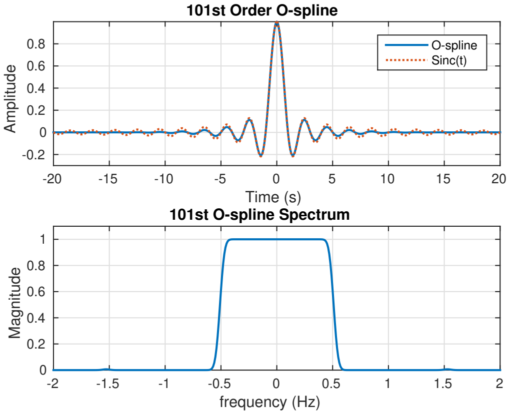

Figure 4: O-spline $K = 101$

For $h = 0$:

$$\begin{aligned} a_0(t_0) &= \xi_0(t_0), & \varphi_0(t_0) &= 0, \\ \dot{a}_0(t_0) &= \dot{\xi}_0(t_0), & \dot{\varphi}_0(t_0) &= 0, \\ \ddot{a}_0(t_0) &= \ddot{\xi}_0(t_0) & \ddot{\varphi}_0(t_0) &= 0. \end{aligned} \tag{27}$$

and for $h > 0$:

$$\begin{aligned} a_h(t_0) &= 2|\xi_h(t_0)|, \\ \varphi_h(t_0) &= \measuredangle \xi_h(t_0), \\ \dot{a}_h(t_0) &= 2\mathrm{Re}\{\dot{\xi}_h(t_0)e^{-j\varphi_h(t_0)}\}, \\ \dot{\varphi}_h(t_0) &= \tfrac{2}{a_h(t_0)}\mathrm{Im}\{\dot{\xi}_h(t_0)e^{-j\varphi_h(t_0)}\}, \\ \ddot{a}_h(t_0) &= 2\mathrm{Re}\{\ddot{\xi}_h(t_0)e^{-j\varphi_h(t_0)}\} + a_h(t_0)\dot{\varphi}_h(t_0)^2, \\ \ddot{\varphi}_0(t_0) &= \tfrac{2}{a_h(t_0)}(\mathrm{Im}\{\ddot{\xi}_h(t_0)e^{-j\varphi_h(t_0)}\} - \dot{a}_h(t_0)\dot{\varphi}_h(t_0)). \end{aligned} \tag{28}$$

Total Phasor Error (TPE)

$$\widehat{x} = \Phi\widehat{\xi} = \Phi\widetilde{\Phi}^H x \tag{29}$$

The Pythagorean theorem holds for the approximation error $e = x - \widehat{x}$, with

$$||e||^2 = ||x||^2 - \widehat{\xi}^H \Phi^H \Phi \widehat{\xi} \tag{30}$$

and normalizing with respect to the signal energy,

$$||\epsilon||^2 = 1 - \frac{\widehat{\xi}^H \Phi^H \Phi \widehat{\xi}}{||x||^2}, \tag{31}$$

Then

$$||\epsilon|| = \sqrt{1 - \frac{\widehat{\xi}^H \Phi^H \Phi \widehat{\xi}}{||x||^2}}. \tag{32}$$

O-splines for $K = 1, \ldots, 11$

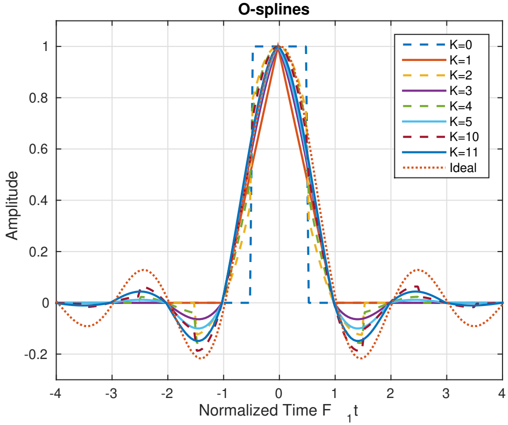

Figure 5: O-splines for $K = 0, 1, \ldots, 5$, 10 and 11.

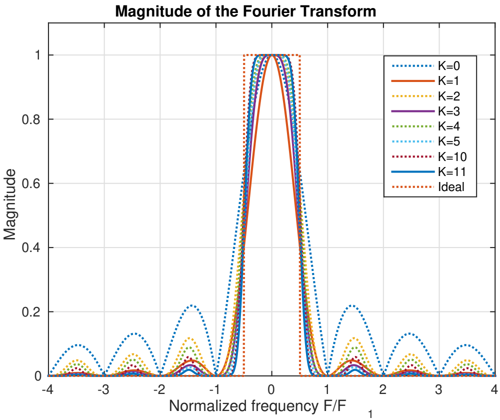

Figure 6: Magnitude of the O-spline Fourier transforms, $K = 0, 1, \ldots, 5$, 10 and 11.

Odd O-spline Spectra

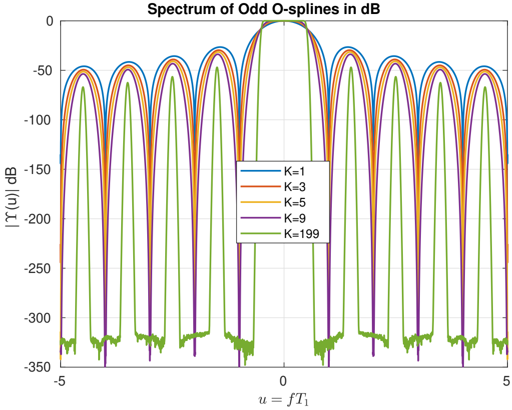

Figure 7: Spectra Odd O-splines, $K = 0, 1, \ldots, 9$, and 199.

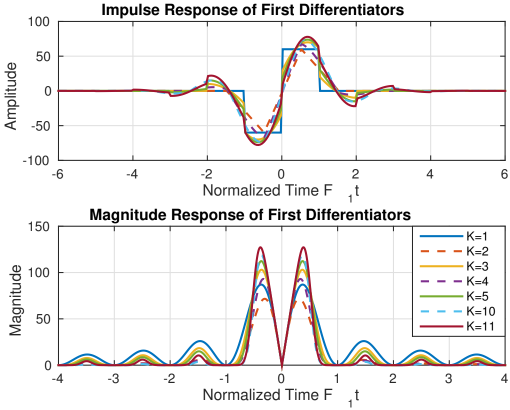

Figure 8: Impulse and magnitude responses of the first differentiators, $K = 0, 1, \ldots, 5$, 10 and 11.

Second Differentiators and their Spectra

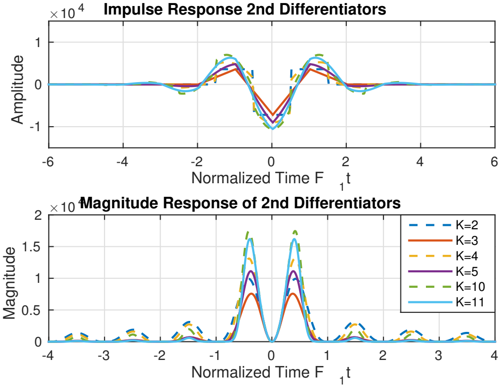

Figure 9: Impulse and magnitude responses of the second differentiators, $K = 0, 1, \ldots, 5$, 10 and 11.

Nonic O-spline Spectrogram of $s(t) = cos(120\pi t + \varphi(t))$ with $\varphi(t) = e^{-4t}\cos(10\pi t)$, and $\dot{\varphi}(t) = -4e^{-4t}\cos(10\pi t) - 10\pi e^{-4t}\sin(10\pi t)$

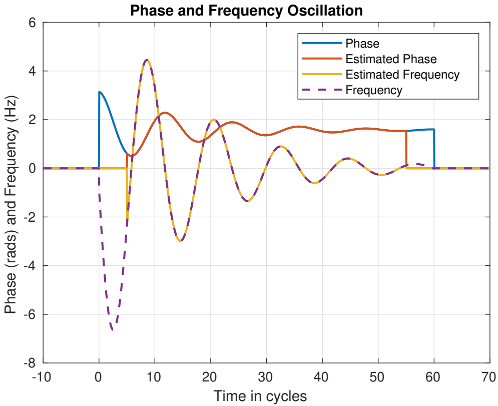

Figure 10: Nonic O-spline Spectogram of $s(t)$.

Analazing Power Oscillations[3]

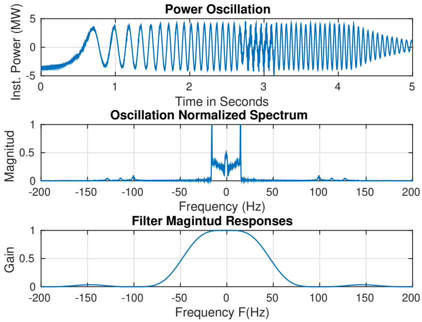

Figure 11: PO (top plot) and its spectrum (middle plot), and frequency response of splitting filters (at the bottom).

[3] J.A. de la O, "Analyzing Power Oscillating Signals with the O-splines of the Discrete Taylor-Fourier Transform", *IEEE Transactions on Power Systems*, vol. 33, no. 6, Nov. 2018, pp. 7087-7095.

Oscillation Spectrogram

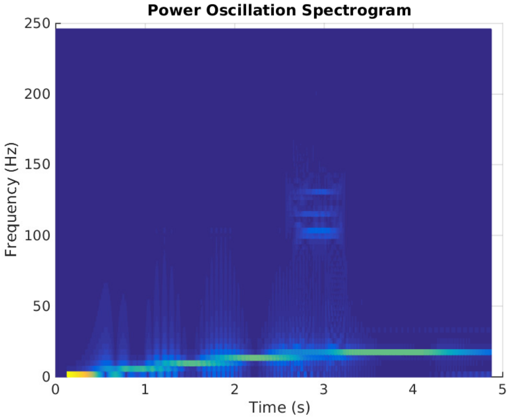

Figure 12: Spectrogram of the oscillation with varying frequency.

Estimated Angle and Frequency Modulations (Spectrogram)

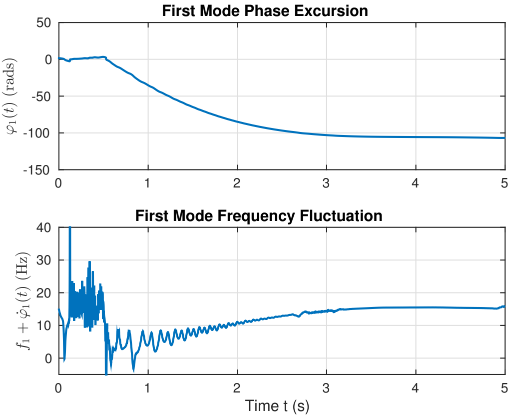

Figure 13: Estimated phase and frequency modulation (Spectrogram).

Analyzed Power Oscillation

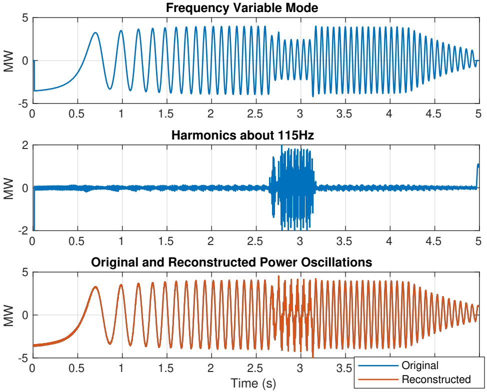

Figure 14: Frequency modulating mode (top plot) and harmonics about 115Hz (middle plot), with the original and reconstructed PO.

Conclusions

- Odd order O-splines are cardinal splines with compact support.
- They offer a ladder of function spaces very useful for multi-resolution analysis.
- They are maximally-flat differentiators that provide state sampling of signals.
- They allow us to estimate not only the signal, but also its instantaneous speed and acceleration.
- Used as bandpass filters, they provide not only the synchrophasor of a signal but also its derivatives, from which amplitude, phase, frequency and ROCOF are obtained.
- They are very useful to analyze modes in power oscillations, with better precision than the Prony method.
- Off course, they are efficient when the signal spectral density is located under the ideal gain of the filters.

Assesing PMU Measurements: Coauthors[4]

(a) Mario Arrieta P.

(b) Alejandro Zamora

Figure 15

[4] J. A. de la O Serna, M. R. Arrieta Paternina, A. Zamora-Mendez, "Assessing Synchrophasor Estimates of an Event Captured by a Phasor Measurement Unit", *IEEE Transactions on Power Delivery*, IEEE Xplore Early Access

Introduction

- Synchrophasor estimates can be evaluated with TVE only for the very few and lax benchmark signals of the Standard.
- This dependence prevents its application to power signals of real events.
- Our research problem is to quantify the erratic phasor estimates provided by a PMU from a real case in a power system.
- The solution of this problem is proposed for obtaining the synchrophasor of real signals.
- A nonic O-spline filter obtains phasor estimates asymptotically close to those obtained with an *ideal bandpass filter*.
- Once the synchrophasor is obtained, the accuracy of one or several PMUs can be assessed using the TVE.
- This solution opens the way to compare synchrophasor estimates of PMUs of different brands, when they process signals of the same power system event.

Convergence to $Sinc(t)$ and $U(F)$

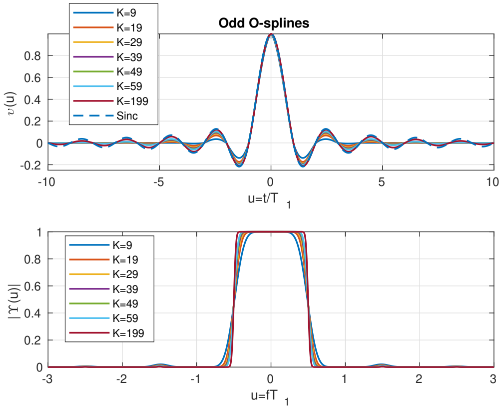

Figure 16: O-spline convergence to $Sinc(t)$, and $U(F)$.

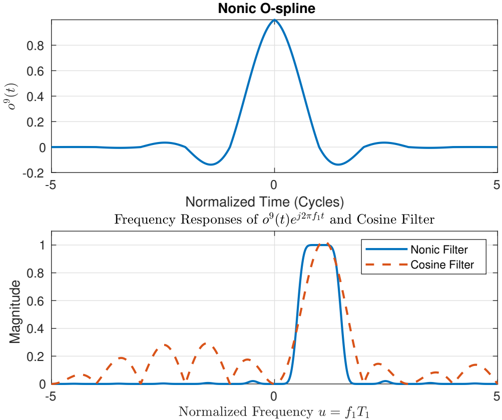

Figure 17: Ten-cycle Nonic O-spline (top plot) used to extract the synchrophasor, and at the bottom its frequency response compared with that of the Cosine filter used in the PMU.

Cauchy Convergence to the Ideal Filter[5]

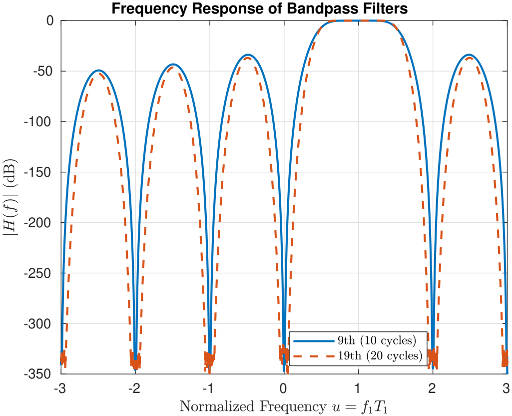

Figure 18: Nonic and decimononic bandpass filters frequency responses.

[5] Distance very small between 9th and 19th O-spline synchrophasors. In a convergent Cauchy sequence, this indicates that their estimates have reached to the ideal synchrophasor.

Filtering Diagram for Synchrophasor Estimates.

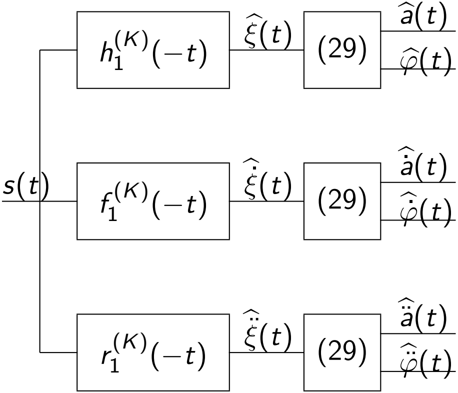

Figure 19: Flowchart of the proposed method.

Steady-State Compliance

Table 1: Steady State Compliance.

Case	**Measurement**	**Standard Limit**
$f_0 \pm 5$ Hz	$TVE = 2.185 \times 10^{-5}$ %	1%
	$\lvert FE \rvert = 0$ Hz	0.005 Hz
	$\lvert RFE \rvert = 5.128 \times 10^{-6}$ Hz/s	0.1 Hz/s
10 % Harmonic distortion up to 50th	$TVE = 2.5 \times 10^{-12}$ %	1 %
	$\lvert FE \rvert = 6 \times 10^{-15}$ Hz	0.025Hz
	$\lvert RFE \rvert = 1.5 \times 10^{-13}$ Hz/s	Limit Suspended
Out-of-Band	$TVE = 2.9933$ %	1.3 %
	$\lvert FE \rvert = 1.166 \times 10^{-05}$ Hz	0.01 Hz
	$\lvert RFE \rvert = 6.9919 \times 10^{-05}$ Hz/s	Limit Suspended

Dynamic Compliance - Measurement Bandwidth.

Table 2: Dynamic Compliance - Measurement Bandwidth.

Case	**Measurement**	**Standard Limit**
Amplitude Modulated	$TVE \leq 2.5 \times 10^{-6}$ %	3 %
	$\lvert FE \rvert \leq 1.95 \times 10^{-7}$ Hz	0.3 Hz
	$\lvert RFE \rvert < 7.357 \times 10^{-6}$ Hz/s	14 Hz/s
Phase Modulated	$TVE \leq 4.71 \times 10^{-5}$ %	3 %
	$\lvert FE \rvert \leq 6.92 \times 10^{-6}$ Hz	0.3 Hz
	$\lvert RFE \rvert < 1.65 \times 10^{-3}$ Hz/s	14 Hz/s.
Frequency Modulated	$TVE \leq 2 \times 10^{-5}$ %	1 %
	$\lvert FE \rvert \leq 1.627 \times 10^{-6}$ Hz	0.01 Hz
	$\lvert RFE \rvert < 5 \times 10^{-4}$ Hz/s	0.2 Hz/s

Dynamic Compliance - Step Responses.

Table 3: Dynamic Complience - Step Responses.

Case	**Measurement**	**Standard Limit**
Amplitude Step	Response time $=$ 7.23 cycles	7 cycles
	delay time $=$ 0 cycles	$\frac{1}{4}$ cycle
	Overshoot $=$ 6.4 %	10 %
	Frequency response time $=$ 6 cycles	14 cycles
	ROCOF response time $=$ 6 cycles	14 cycles
Phase Step	Response time $=$ 7.37 cycles	7 cycles
	delay time $=$ 0 cycles	$\frac{1}{4}$ cycle
	Overshoot $=$ 7.4 %	10 %
	Frequency response time $=$ 6 cycles	14 cycles
	ROCOF response time $=$ 8 cycles	14 cycles
Modulated Frequency	$TVE \leq 2 \times 10^{-5}$ %	1 %
	$\lvert FE \rvert \leq 1.627 \times 10^{-6}$ Hz	0.01 Hz
	$\lvert RFE \rvert < 5 \times 10^{-4}$ Hz/s	0.2 Hz/s

Study Case: Event in System with Solar and Wind Power Generation

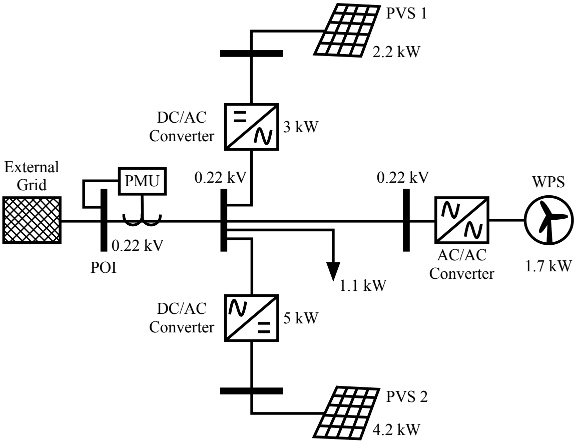

Figure 20: Topology of the low-voltage distributed generation system considered in this paper with two PVSs and one WPS interconnected to the grid.

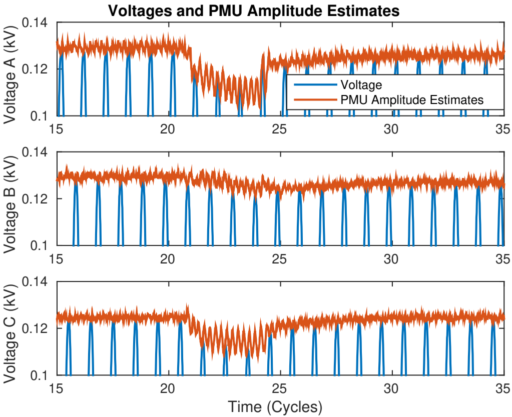

Figure 21: Voltage waveforms with amplitude estimated by the PMU.

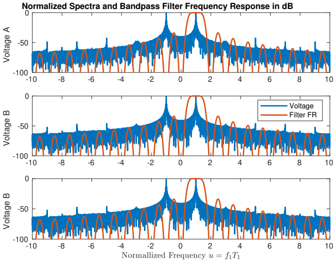

(a) Spectra and fundamental bandpass filter

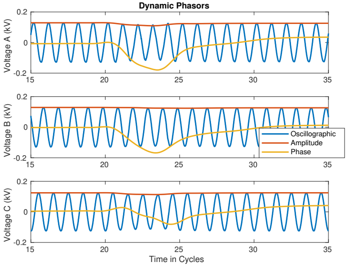

(b) Dynamic Phasors.

Figure 22: Voltage spectra and nonic DTTFT filter frequency response. At the bottom, voltage oscillography and the corresponding synchrophasors.

Current Spectra

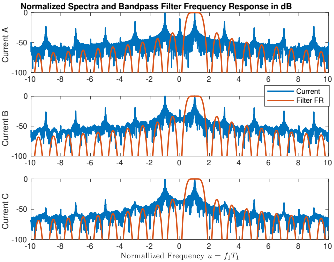

(a) Spectra and fundamental bandpass filter

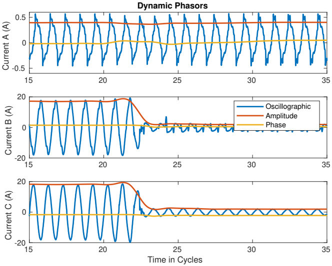

(b) Dynamic Phasors.

Figure 23: Current spectra and nonic DTTFT filter frequency response. At the bottom, current oscillography and the corresponding synchrophasors (amplitude and phase).

Current and their synchrophasor syntetic signals

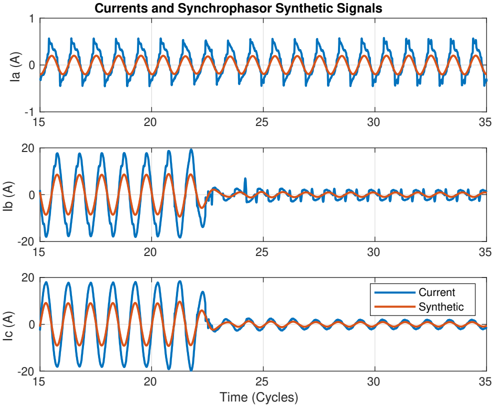

Figure 24: Currents and their synchrophasor synthetic signals.

Current Phasor Estimates

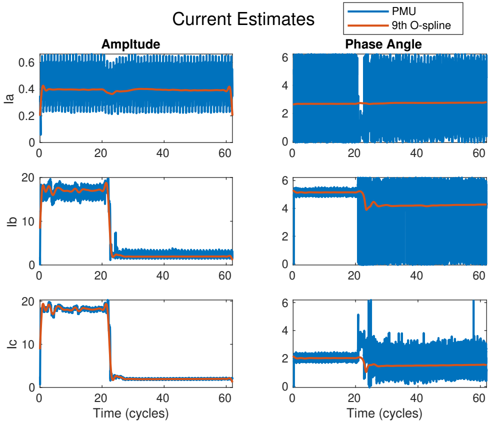

Figure 25: Current phasor estimates. At the left column the amplitudes, and at the right column the corresponding phase angles.

TVE of PMU Voltage Estimates

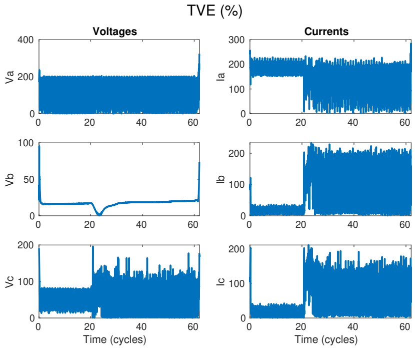

Figure 26: TVE of PMU Voltage (left), and current (right) estimates.

Frequency and ROCOF Estimaes from Voltages

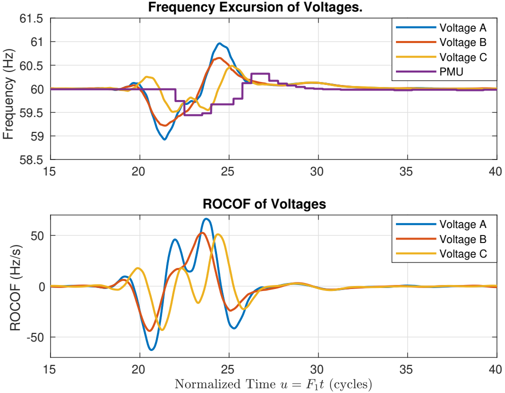

Figure 27: Frequency and ROCOF estimates from voltage channels obtained with the nonic O-spline first and second differentiators.

Discussion I: What Standards Are [6]

- Standards reflect the global *consensus* and *distilled wisdom* of many technical delegated experts.
- They provide instructions, guidelines, rules or definitions that are used to *design, manufacture, install, test & certify, maintain and repair electrical and electronic* devices and systems.
- They are essential for quality and risk management;
- Standards are always used by voluntary technical experts (and based on *international consensus*).
- They help researchers to understand the value of innovation and allow *manufacturers* to produce products of *consistent quality and performance*.

[6] Taken from: `https://www.iec.ch/understanding-standards`

Discussion II: Synchrophasor Standard IEC/IEEE 60255-118-1

- Standards are not for promoting scientific *research*, it is the other way around.
- The O-spline performance shows that the standard limits are unduly lax.
- The standard prevents to test PMUs with real signals whose synchrophasors are unknown.
- TVE only takes into account amplitude and phase. A synthetic error including frequency and ROCOF is required.
- Out-of-Band test obliges to filter out important oscillations due to a low reportig rate.
- The standard allows noisy frequency and ROCOF estimates.

Scalar and Wavelet Functions: Meyer and de la O nonic and decimononic.

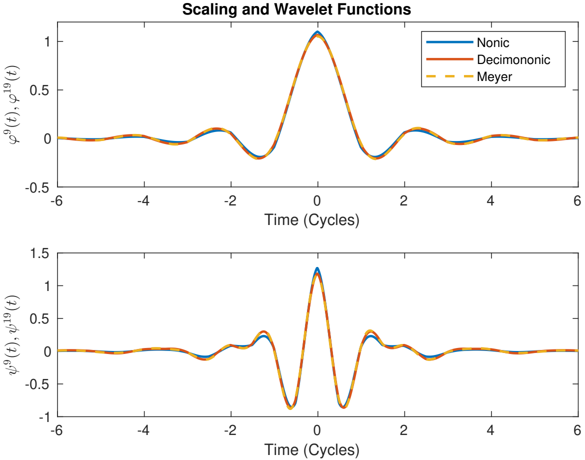

Figure 28: Scaling functions and Wavelets: Meyer and de la O nonic and decimononic.

Scalar and Wavelet Functions: Bandlimited and de la O^∞.

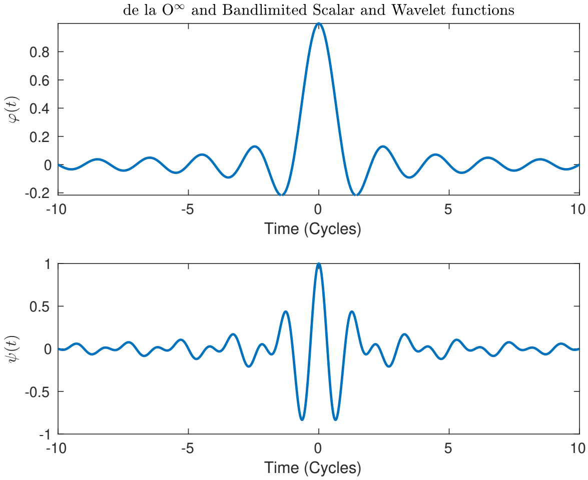

Figure 29: Scaling functions and Wavelets: Bandlimited and de la O^∞.

Mathematicians involved in this work

- Johann Carl Friedrich **Gauss**
- Leonhard **Euler**
- Joseph **Fourier**
- Brook **Taylor**
- Gaspard Richard **de Prony**
- David **Hilbert**
- Marc Antoine **Parseval**, Friedrich Wilhelm **Bessel**, Brian Lewis **Butterworth**, Pafnuty **Chebyshev**
- Rudolf E. **Kalman**
- Yves **Meyer**, Stéphan **Mallat**, Ingrid **Daubechys**, Jalena **Kovačević**, Martin **Vetterli**, David **Walnut**.

Conclusions

- The paper proposes a quantitative method to assess the estimation performance of PMUs using signals from the field, instead of only with the few benchmark signals of the Standard.
- Real signals contain realistic harmonics and real noisy conditions.
- The analyzed case exhibits very poor and erratic PMU estimates, with intolerable TVEs.
- This work opens up the possibility of employing the TVE to assess and compare the estimation performance of different PMUs at a control center, when they monitor the same disturbance.
- Application that was considered before as unthinkable and impossible.

Bibliografía

1. J. A. de la O Serna, M. R. Arrieta Paternina, A. Zamora-Mendez, "Assessing Synchrophasor Estimates of an Event Captured by a Phasor Measurement Unit", *IEEE Transactions on Power Delivery*, IEEE Xplore Early Access: 26 Oct 2020.
2. J. A. de la O Serna, "Dynamic Harmonic Analysis with FIR filters designed with O-splines", *IEEE Transactions on Circuits and Systems I: Regular Papers*, Vol.67, No.12, Dec. 2020, pp. 5092-5100.
3. J.A. de la O, "Analyzing Power Oscillating Signals with the O-splines of the Discrete Taylor-Fourier Transform", *IEEE Transactions on Power Systems*, vol. 33, no. 6, Nov. 2018, pp. 7087-7095.

Thanks.

jdelao@ieee.org